PAPER

The interaction of transverse domain walls

IOP PUBLISHING JOURNAL OF PHYSICS: CONDENSED MATTER

J. Phys.: Condens. Matter **24** (2012) 024209 (9pp) doi:10.1088/0953-8984/24/2/024209

The interaction of transverse domain walls

Benjamin Krüger

I. Institut für Theoretische Physik, Universität Hamburg, Jungiusstraße 9, 20355 Hamburg, Germany

E-mail: bkrueger@physnet.uni-hamburg.de

Received 1 June 2011, in final form 5 August 2011
Published 15 December 2011
Online at stacks.iop.org/JPhysCM/24/024209

Abstract

The interaction between transverse domain walls is calculated analytically using a multipole expansion up to third order. Starting from an analytical expression for the magnetization in the wall, the monopole, dipole, and quadrupole moments are derived and their impact on the interaction is investigated using the surface and volume charges. The surface charges are important for the dipole moment while the volume charges constitute the monopole and quadrupole moments. For domain walls that are situated in different wires it is found that there is a strong deviation from the interaction of two monopoles. This deviation is caused by the interaction of the monopole of the wall in the first wire with the dipole of the wall in the second wire and vice versa. The dipole–dipole and the quadrupole–monopole interactions are found to be also of considerable size and non-negligible. A comparison with micromagnetic simulations shows a good agreement.

(Some figures may appear in colour only in the online journal)

1. Introduction

The observation that a current that is traversing a magnetic sample may alter the magnetic configuration [1–6] triggered an intensive investigation of the interplay between currents, magnetic fields, and the magnetization in nanostructured samples.

Recently memory devices have been proposed that consist of magnetic domain walls that are beaded along a magnetic nanowire. A current flowing in the wire can be used to shift these walls passing a reading and a writing device [7]. For a high storage density the magnetic nanowires have to be close to each other and for a reliable description of the dynamics it is important to take the interaction with other walls into account.

If the two interacting domain walls have a sizable distance between them there is no exchange interaction and the interaction via the demagnetization energy can be expanded in a series of multipoles. On discarding their internal structure, the interaction of two domain walls can be modeled by an interaction of two monopoles. Numerical simulations of domain walls in neighboring wires that are close together showed that this is a good approximation for vortex walls but for transverse walls it is not sufficient [8, 9]. It was proposed that this discrepancy between numerical simulations and the monopole model is due to a dipole–dipole coupling between the transverse magnetization components in both walls [9].

In this work the interaction between two walls is calculated analytically, taking the monopole–monopole, dipole–monopole, dipole–dipole, and quadrupole–monopole interactions into account. Using an analytical expression for the magnetization in the domain walls [10], the monopole, dipole, and quadrupole moments of a transverse domain wall are calculated by using the so called surface and volume charges. The surface charges depend on the normal component of the magnetization at the surfaces of the wire and are important for the dipole moment. The volume charges depend on the divergence of the magnetization and constitute the monopole and quadrupole moments. The results are compared with micromagnetic simulations.

This work is organized as follows. In section 2 the equation of motion of a single domain wall is discussed. In section 3 it is discussed how the equation of motion can be expanded to account for the interaction between different domain walls. For this purpose the interaction energy of two walls is calculated. Sections 4 and 5 deal with the special cases where the two walls are located in the same wire and where

the two walls are located in different wires, respectively. The results for the latter case are compared with micromagnetic simulations in section 6. Finally a conclusion is given.

2. The equation of motion

In this section the dynamics of the domain wall is described using a one-dimensional model, i.e., the magnetization depends only on the position x along the wire. In the following, θ denotes the angle between the magnetization and the wire axis. χ is the angle of the magnetization around the wire axis as illustrated in figure 1. In the wall there are two competing energies. The exchange energy $A\int \mathrm{d}V[(\partial\theta/\partial x)^2+\sin^2(\theta)(\partial\chi/\partial x)^2]$ with the exchange constant A tends to align neighboring magnetic moments parallel to each other. The anisotropy energy $K\int \mathrm{d}V\sin^2(\theta)$, where K is the strength of the anisotropy, is lower when the magnetization points in the wire direction. The sum of the two energies is minimized for an angle χ that is uniform along the wire and an angle θ that is given by

$$\cos(\theta) = -a\tanh\left(\frac{x-X}{\lambda}\right) \qquad \text{and} \qquad \sin(\theta) = \frac{1}{\cosh(\frac{x-X}{\lambda})}. \tag{1}$$

Here, X is the position of the center of the wall, $\lambda=\sqrt{A/K}$ is the width of the wall, and a distinguishes between a head-to-head wall ($a=+1$) and a tail-to-tail wall ($a=-1$; see figure 1). The domain wall moves like a composite particle [11] and it is possible to derive the equations of motion [12, 10]

$$\dot{X} = -\frac{\gamma'\alpha\lambda}{2S\mu_0 M_\mathrm{s}}\frac{\partial E}{\partial X} + \frac{a\gamma'}{2S\mu_0 M_\mathrm{s}}\frac{\partial E}{\partial \chi} - (1+\alpha\xi)b_j' j \tag{2}$$

for the center of the wall and

$$\dot{\chi} = -\frac{a\gamma'}{2S\mu_0 M_\mathrm{s}}\frac{\partial E}{\partial X} - \frac{\gamma'\alpha}{2S\mu_0 M_\mathrm{s}\lambda}\frac{\partial E}{\partial \chi} - a\frac{\xi-\alpha}{\lambda}b_j' j \tag{3}$$

for the angle of the magnetization in the wall. Here $S=wd$ is the cross section of the wire, α is the Gilbert damping parameter, ξ is the strength of the non-adiabatic spin torque, γ is the gyromagnetic ratio, M_s is the saturation magnetization, and b_j is the strength of the coupling between the current density j and the magnetization. In equations (2) and (3) the abbreviations $\gamma'=\gamma/(1+\alpha^2)$ and $b_j'=b_j/(1+\alpha^2)$ have been used.

With the energy density given above, the wall is able to rotate freely around the wire; thus for a wire with a non-circular cross section one adds a second anisotropy term $K_\perp\sin^2(\theta)\sin^2(\chi)$ that describes a hard axis perpendicular to the wire. The introduction of an external magnetic field in the direction of the wire yields the additional term $-\mu_0 M_\mathrm{s} H_\mathrm{ext}\cos(\theta)$. A pinning potential in the wire is described by a pinning energy $E_\mathrm{pin}(X,\chi)$. With the aid of equation (1) one finds the additional energy

$$E = 2S\lambda K_\perp\sin^2(\chi) - 2Sa\mu_0 M_\mathrm{s} H_\mathrm{ext} X + E_\mathrm{pin}(X,\chi), \tag{4}$$

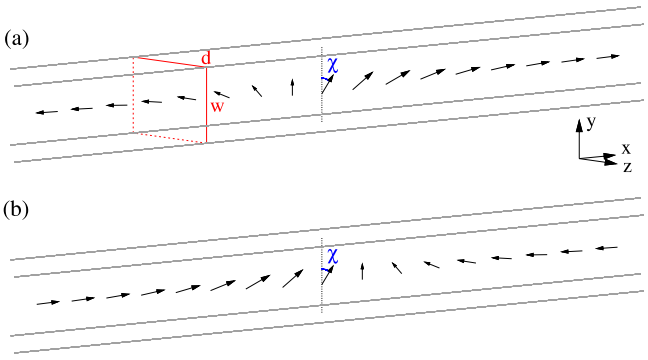

Figure 1. Scheme of the magnetization (arrows) of two transverse walls in a nanowire with width w and thickness d. The parameter a, that is the sign of the volume charges of the wall, distinguishes between (a) a tail-to-tail ($a=-1$) and (b) a head-to-head ($a=+1$) domain wall. The orientation of the perpendicular magnetization, that is important for the surface charges of the wall, is given by the angle χ.

which includes all three terms. Inserting this energy into equations (2) and (3) one ends up with

$$\dot{X} = \frac{a\lambda\sin(2\chi)}{2\alpha\tau_d} - \frac{\alpha^2\tau_d}{m}\frac{\partial E_\mathrm{pin}}{\partial X} + \frac{a\alpha\tau_d}{m\lambda}\frac{\partial E_\mathrm{pin}}{\partial\chi} + \frac{\lambda\kappa_1}{\tau_d} \tag{5}$$

for the position and

$$\dot{\chi} = -\frac{\sin(2\chi)}{2\tau_d} - \frac{a\alpha\tau_d}{m\lambda}\frac{\partial E_\mathrm{pin}}{\partial X} - \frac{\alpha^2\tau_d}{m\lambda^2}\frac{\partial E_\mathrm{pin}}{\partial\chi} + \frac{a\alpha\kappa_2}{\tau_d}, \tag{6}$$

for the angle of the wall. Here, the intrinsic damping time $\tau_d=\mu_0 M_\mathrm{s}/(2\gamma' K_\perp\alpha)$ and the mass $m=S\mu_0^2 M_\mathrm{s}^2/(\gamma'^2 K_\perp\lambda)$ of the domain wall have been used [10, 13]. The dimensionless abbreviations κ_1 and κ_2 describe the strength of the excitation due to the current and the field. They are defined as $\kappa_1 = a\alpha\tau_d\gamma' H_\mathrm{ext} - (1+\alpha\xi)\tau_d b_j' j/\lambda$ and $\kappa_2 = a\tau_d\gamma' H_\mathrm{ext}/\alpha - (\xi/\alpha - 1)\tau_d b_j' j/\lambda$.

In the absence of a pinning potential and for a constant field and a constant current, equation (6) has the solution

$$\frac{\sin(2\chi)}{2} = \frac{a}{2}\frac{1\pm 2\alpha\kappa_2\cos(\omega_\chi t)}{2\alpha\kappa_2\pm\cos(\omega_\chi t)} \tag{7}$$

with $\omega_\chi=\sqrt{4\alpha^2\kappa_2^2-1}/\tau_d$. For small excitations ($2\alpha|\kappa_2|<1$) there is an equilibrium value for χ with $\sin(2\chi_\mathrm{eq})=2a\alpha\kappa_2$, while for large excitations ($2\alpha|\kappa_2|>1$) the wall performs a continuous rotation around the wire axis. By inserting this solution in equation (5) it is possible to derive the velocity of the wall. For small excitations this velocity is

$$\dot{X}_\mathrm{eq} = \frac{\lambda(\kappa_1+\kappa_2)}{\tau_d} \tag{8}$$

when χ has reached its equilibrium value. For $2\alpha|\kappa_2|>1$ the velocity changes with time. For increasing excitations its average value

$$\dot{X}_\mathrm{av} = \frac{\lambda(\kappa_1+\kappa_2)}{\tau_d} - \frac{\lambda\kappa_2}{\tau_d}\frac{\tau_d\omega_\chi}{\sqrt{\tau_d^2\omega_\chi^2+1}} \tag{9}$$

changes continuously from $\lambda(\kappa_1 + \kappa_2)/\tau_d$ to $\lambda\kappa_1/\tau_d$ as calculated by Hayashi *et al* [14]. The limiting case for large excitations has also been derived by Mougin *et al* [15].

In the presence of pinning potentials, equations (5) and (6) are solved numerically [12, 16, 13, 17, 18]. These solutions have been found to reproduce the experimental results very well and have proven to be helpful in the interpretation [12, 16, 13, 17]. Furthermore, this model was also successful in predicting new effects in the dynamics of a single domain wall [18]. If more than one domain wall is involved in the dynamics, the interactions between two walls have to be taken into account to obtain a reliable prediction of the motion of the walls.

3. Domain wall interaction

For one domain wall the wall moves in a potential E_{pin} that is given by pinning centers in the wire. For systems with more domain walls the potential for each wall is influenced by the presence of the other walls. Thus the dynamics of the wall can be derived by adding the interaction energy to E_{pin} in equations (5) and (6). This interaction can be between domain walls in neighboring wires that are close together or between two walls in the same wire. The interaction energy is calculated in the following.

The demagnetization energy of the whole sample is given by

$$E_{\text{D}} = \frac{\mu_0}{8\pi} \int (\mathrm{d}V\, \rho_{\text{v}}(\vec{r}) + \mathrm{d}A\, \sigma_{\text{s}}(\vec{r})) \times \int (\mathrm{d}V'\, \rho_{\text{v}}(\vec{r}') + \mathrm{d}A'\, \sigma_{\text{s}}(\vec{r}')) \frac{1}{|\vec{r} - \vec{r}'|} \tag{10}$$

with the volume charges

$$\rho_{\text{v}}(\vec{r}) = -\vec{\nabla}\vec{M}(\vec{r}) \tag{11}$$

and surface charges

$$\sigma_{\text{s}}(\vec{r}) = \vec{M}(\vec{r})\vec{n}(\vec{r}), \tag{12}$$

where $\vec{n}(\vec{r})$ is the normal vector of the surface at position $\vec{r}$. These charges are depicted in figure 2. In the following all terms that are independent of the distance apart of the walls are neglected. The interaction energy of two walls is then given as

$$E = \frac{\mu_0}{4\pi} \int (\mathrm{d}V_1\, \rho_{\text{v}1}(\vec{r}_1) + \mathrm{d}A_1\, \sigma_{\text{s}1}(\vec{r}_1)) \times \int (\mathrm{d}V_2\, \rho_{\text{v}2}(\vec{r}_2) + \mathrm{d}A_2\, \sigma_{\text{s}2}(\vec{r}_2)) \frac{1}{|\vec{R} + \vec{r}_2 - \vec{r}_1|} \tag{13}$$

where $\vec{r}_1$ and $\vec{r}_2$ are the positions with respect to the center of the first and second domain walls, respectively. The distance vector $\vec{R}$ points from the center of the first wall to the center of the second wall. V_1 and V_2 are the volumes of the first and second domain walls, respectively. A_1 and A_2 represent the respective surfaces. In the following it is assumed that both walls are situated in nanowires that are aligned along the x direction. Then equation (13) can be written as

$$E = \frac{\mu_0}{4\pi} \int \mathrm{d}V_1\, \rho_1(\vec{r}_1) \int \mathrm{d}V_2\, \rho_2(\vec{r}_2) \frac{1}{|\vec{R} + \vec{r}_2 - \vec{r}_1|} \tag{14}$$

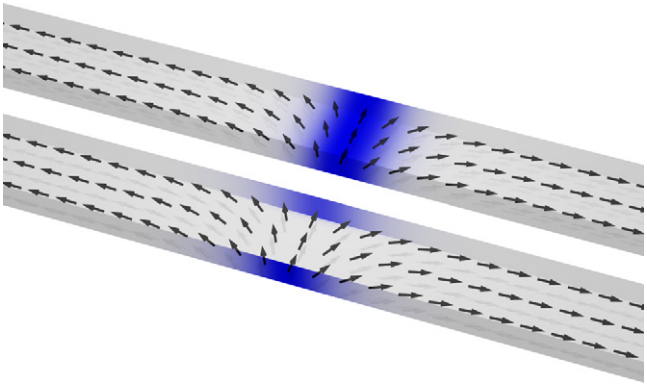

Figure 2. Scheme of the volume (upper wire) and the surface charges (lower wire) of a transverse wall in a wire with a rectangular cross section. The absolute values of the charges are given by the color gradient. The arrows denote the magnetization.

with the charge density

$$\rho_i(\vec{r}) = \frac{a_i M_{\text{s}}}{\lambda_i \cosh^2(\frac{x}{\lambda_i})} \Theta\left(\frac{w_i}{2} - |y|\right) \Theta\left(\frac{d_i}{2} - |z|\right) + \cos(\chi_i) M_{\text{s}} \frac{\delta(y - \frac{w_i}{2}) - \delta(y + \frac{w_i}{2})}{\cosh(\frac{x}{\lambda_i})} \Theta\left(\frac{d_i}{2} - |z|\right) + \sin(\chi_i) M_{\text{s}} \frac{\delta(z - \frac{d_i}{2}) - \delta(z + \frac{d_i}{2})}{\cosh(\frac{x}{\lambda_i})} \Theta\left(\frac{w_i}{2} - |y|\right) \tag{15}$$

that includes volume and surface charges. Here the analytical expressions for the magnetization that are given in equation (1) are used. The surface integrals are translated to volume integrals with the aid of a δ-function. $\Theta(x)$ is the Heaviside step function. w_i and d_i denote the width and thickness of the wire in which the ith domain wall is situated, respectively. The constant a_i and the angle χ_i describe the magnetization in the ith domain wall as depicted in figure 1. The term that depends on a_i denotes the volume charges and the terms that depend on χ_i denote the surface charges. For a head-to-head wall the volume charges are positive. For a tail-to-tail wall the volume charges are negative. The angle χ_i describes the location of the surface charges. This location changes when the magnetization in the domain wall rotates around the wire axis. The energy given in equation (14) is valid as long as the volumes V_1 and V_2 of the two walls do not overlap. However, one has to keep in mind that the charge density is derived from equation (1), i.e. using the approximation of a one-dimensional model.

For $|\vec{r}_1| \ll |\vec{R}|$ and $|\vec{r}_2| \ll |\vec{R}|$ one is able to expand the interaction in equation (14) in a series of multipoles. A Taylor series up to second order in $\vec{r}_1$ and $\vec{r}_2$ at $\vec{r}_1 = 0$ and $\vec{r}_2 = 0$ yields

$$E \approx \frac{\mu_0}{4\pi|\vec{R}|} q_1 q_2 + \frac{\mu_0}{4\pi|\vec{R}|^3} (\vec{p}_1 q_2 - q_1 \vec{p}_2)\vec{R} + \frac{\mu_0}{8\pi|\vec{R}|^5} \vec{R}(2(\vec{p}_1\vec{p}_2)\mathbb{1} - 6\vec{p}_1 \otimes \vec{p}_2 + Q_1 q_2 + q_1 Q_2)\vec{R}, \tag{16}$$

where q_i, p_i, and Q_i are the monopole, dipole, and quadrupole moments of the ith wall, respectively.

In the following it is assumed for simplicity that the two domain walls are in wires that have the same width w and thickness d. Since the width λ of the wall depends only on material parameters and the cross section of the wire, the widths of the two walls are the same. The monopole of the ith wall is

$$q_i = 2M_s a_i S. \tag{17}$$

Here, $S = wd$ is the cross section of the wire. The dipole and quadrupole moments are given by

$$\vec{p}_i = M_s S \pi \lambda (0, \cos(\chi_i), \sin(\chi_i)) \tag{18}$$

and

$$Q_i = M_s \frac{a_i S}{6} \times \begin{pmatrix} 2\pi^2\lambda^2 - w^2 - d^2 & 0 & 0 \\ 0 & 2w^2 - \pi^2\lambda^2 - d^2 & 0 \\ 0 & 0 & 2d^2 - \pi^2\lambda^2 - w^2 \end{pmatrix}. \tag{19}$$

With these multipole moments one is able to expand the interaction energy in terms of $1/R$ with $R = |\vec{R}|$. The first order is given by the interaction between the two monopole terms. The corresponding energy is

$$E_{qq} = \frac{\mu_0 M_s^2 S^2}{\pi R} a_1 a_2. \tag{20}$$

The second order is the interaction between the monopole of the first wall with the dipole of the second wall and vice versa. This energy is then given as

$$E_{pq} = \frac{\mu_0 M_s^2 S^2}{2R^3} \lambda a_1 a_2 (R_y (a_1 \cos(\chi_1) - a_2 \cos(\chi_2)) + R_z (a_1 \sin(\chi_1) - a_2 \sin(\chi_2))). \tag{21}$$

The next order consists of two terms, that are the dipole–dipole and quadrupole–monopole interactions. The dipole–dipole term is

$$E_{pp} = \frac{\mu_0 M_s^2 S^2}{4R^5} \pi\lambda^2 (R^2 - 3R_y^2) \cos(\chi_1)\cos(\chi_2) + \frac{\mu_0 M_s^2 S^2}{4R^5} \pi\lambda^2 (R^2 - 3R_z^2) \sin(\chi_1)\sin(\chi_2) - 3\frac{\mu_0 M_s^2 S^2}{4R^5} \pi\lambda^2 R_y R_z (\cos(\chi_1)\sin(\chi_2) + \sin(\chi_1)\cos(\chi_2)). \tag{22}$$

The energy of the quadrupole–monopole interaction can be calculated as

$$E_{Qq} = \frac{\mu_0 M_s^2 S^2}{12\pi R^5} ((2\pi^2\lambda^2 - w^2 - d^2) R_x^2 + (2w^2 - \pi^2\lambda^2 - d^2) R_y^2 + (2d^2 - \pi^2\lambda^2 - w^2) R_z^2) a_1 a_2. \tag{23}$$

The energies in equations (20)–(23) have to be added to the energy of the wall that is used in equations (5) and (6). Thus the interaction has an influence on the domain wall dynamics.

The interaction energy should be invariant under a rotation of the sample by 180° around the x axis with a renumbering of the walls and under an inversion of the magnetization. The rotation is equivalent to the substitutions

$$a_1 \to a_2, \quad a_2 \to a_1, \quad \chi_1 \to \chi_2 + \pi, \quad \chi_2 \to \chi_1 + \pi, \quad \text{and} \quad R_x \to -R_x. \tag{24}$$

Here R_y and R_z remain the same because both the rotation and the renumbering change their sign. The inversion of the magnetization is equivalent to the substitutions

$$a_1 \to -a_1, \quad a_2 \to -a_2, \quad \chi_1 \to \chi_1 + \pi, \quad \text{and} \quad \chi_2 \to \chi_2 + \pi. \tag{25}$$

Obviously, equations (20)–(23) are invariant under the above substitutions.

4. Domain walls in the same wire

If both domain walls are in the same wire, $R_y = R_z = 0$. Thus the dipole–monopole interaction vanishes. The remaining contributions to the interaction energy become

$$E_{qq} = \frac{\mu_0 M_s^2 S^2}{\pi R} a_1 a_2 \tag{26}$$

for the monopole–monopole interaction,

$$E_{pp} = \frac{\mu_0 M_s^2 S^2}{4R^3} \pi\lambda^2 \cos(\chi_1 - \chi_2) \tag{27}$$

for the dipole–dipole interaction, and

$$E_{Qq} = \frac{\mu_0 M_s^2 S^2}{12\pi R^3} (2\pi^2\lambda^2 - w^2 - d^2) a_1 a_2, \tag{28}$$

for the quadrupole–monopole interaction. Thus the interaction energy is

$$E_{WW} = \frac{\mu_0 M_s^2 S^2 a_1 a_2}{\pi R} \times \left(1 + \frac{\pi^2\lambda^2 (2 + 3a_1 a_2 \cos(\chi_1 - \chi_2)) - w^2 - d^2}{12R^2}\right) \tag{29}$$

where the second term in brackets describes the deviation from the pure monopole model.

5. Domain walls in neighboring wires

For two domain walls that are located in neighboring wires the dipole–monopole interaction may be finite. In the following the distance between the centers of the wires points in the y direction and is denoted by D. The maximum contribution of the dipole–monopole energy is obtained if $|\cos(\chi_1)| = |\cos(\chi_2)| = 1$. In this case the magnetization for both walls lies in the xy plane as depicted in figure 3. The interaction energy of two walls that have the smallest possible distance between them is calculated by setting $R_x = R_z = 0$ and $R_y = D$

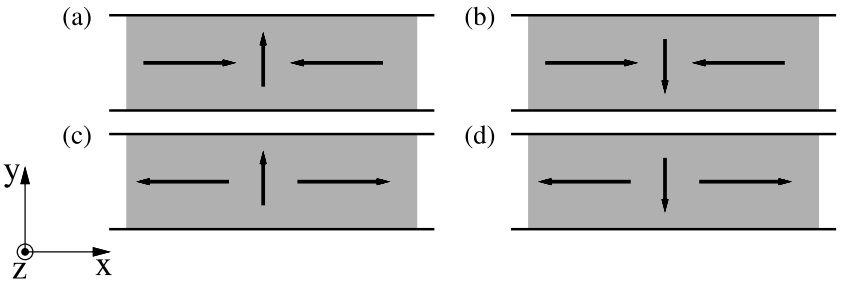

Figure 3. Schemes of the four different magnetic configurations of a domain wall with a magnetization that lies in the *xy* plane. The figure shows domain walls with (a) $a = +1$ and $\cos(\chi) = +1$, (b) $a = +1$ and $\cos(\chi) = -1$, (c) $a = -1$ and $\cos(\chi) = +1$, and (d) $a = -1$ and $\cos(\chi) = -1$.

in equations (20)–(23). With these assumptions for the angles and the distance, the energies reduce to

$$E_{qq} = \frac{\mu_0 M_s^2 S^2}{\pi D} a_1 a_2 \tag{30}$$

for the monopole–monopole interaction,

$$E_{pq} = \frac{\mu_0 M_s^2 S^2}{2D^2} \lambda a_1 a_2 (a_1 c_1 - a_2 c_2) \tag{31}$$

for the dipole–monopole interaction,

$$\begin{aligned} E_{pp} &= -\frac{\mu_0 M_s^2 S^2}{2D^3} \pi \lambda^2 c_1 c_2 \\ &= -\frac{\mu_0 M_s^2 S^2}{2D^3} \pi \lambda^2 a_1 a_2 \left(1 - \frac{(a_1 c_1 - a_2 c_2)^2}{2}\right) \end{aligned} \tag{32}$$

for the dipole–dipole interaction, and

$$E_{Qq} = \frac{\mu_0 M_s^2 S^2}{12\pi D^3} (2w^2 - \pi^2 \lambda^2 - d^2) a_1 a_2, \tag{33}$$

for the quadrupole–monopole interaction. Here the abbreviations $c_1 = \cos(\chi_1)$ and $c_2 = \cos(\chi_2)$ are used. The interaction energy is given by

$$\begin{aligned} E_{WW} = \frac{\mu_0 M_s^2 S^2 a_1 a_2}{\pi D} \Bigg(1 + \frac{\pi \lambda (a_1 c_1 - a_2 c_2)}{2D} \\ + \frac{2w^2 - \pi^2 \lambda^2 (7 - 3(a_1 c_1 - a_2 c_2)^2) - d^2}{12D^2}\Bigg). \end{aligned} \tag{34}$$

The second and third term in brackets describe the deviation from the monopole model. It is worth noting that the first term is of first order in $1/D$, in contrast to the case where the two domain walls are in the same wire. A maximum attractive interaction is found for $a_1 a_2 = -1$ and $a_1 c_1 - a_2 c_2 = +2$. The dependence of the energy of the spacing between the wires is depicted in figure 4.

6. Numerical calculations

For a comparison of the analytical expression in equation (34) with numerical calculations a system that consists of two parallel wires of length l and distance apart D is simulated using the object oriented micromagnetic framework (OOMMF) [19]. For these simulations, wires with rectangular cross section with $w = 100$ nm and $d = 10$ nm are used. The simulations are performed using the material parameters of permalloy, which are $A = 1.3 \times 10^{-11}$ J m^{-1} and $M_s = 8 \times 10^5$ A m^{-1}. The cell size is 1 nm in the x and y directions and 10 nm in the z direction. A sketch of the interactions in this system is shown in figure 5. The magnetization at the four wire ends is kept constant in the direction of the wire. This ensures that no end domains are formed and the energy of the ends of the wire can be calculated analytically.

From the expression calculated in equation (1) one finds

$$m_\perp = M_s S \pi \lambda \tag{35}$$

for the magnetic moment $m_\perp$ perpendicular to the wire. In turn this allows for a calculation of λ from the numerically obtained value $m_\perp = 5.75 \times 10^{-17}$ A m^2. This leads to a width of the domain walls of $\lambda = 22.9$ nm.

The energy of this system is

$$\begin{aligned} E(l, D) = 2E_W + E_{WW}(a_1, a_2, c_1, c_2, D) - 4E_{W1}(l) \\ + 4E_{W2}(l, D) + 4E_{WE} - 2E_{EE}(D) + 2E_{E1}(l) \\ - 2E_{E2}(l, D) \end{aligned} \tag{36}$$

where E_W is the self-energy of one domain wall,

$$E_{WE} = \frac{\mu_0 M_s^2 d^3}{4\pi} F_N\left(\frac{w}{d}\right) \tag{37}$$

is the energy of one of the four wire ends [20],

$$\begin{aligned} E_{EE} = \frac{\mu_0 M_s^2 d^3}{4\pi} \left(F_N\left(\frac{D+w}{d}\right) + F_N\left(\frac{D-w}{d}\right)\right. \\ \left. - 2F_N\left(\frac{D}{d}\right)\right), \end{aligned} \tag{38}$$

with $D > w$ and

$$\begin{aligned} F_N(x) = x \ \operatorname{arcsinh}(x) + x^2 \operatorname{arcsinh}\left(\frac{1}{x}\right) \\ + \frac{x^3 + 1 - \sqrt{1 + x^2}^3}{3}, \end{aligned} \tag{39}$$

is the interaction energy of adjacent ends of different wires [20], and E_{WW} is the energy of interaction between the two domain walls. The remaining terms are the interaction energies as depicted in figure 5. The expressions in equations (37) and (38) can be derived from equation (10),

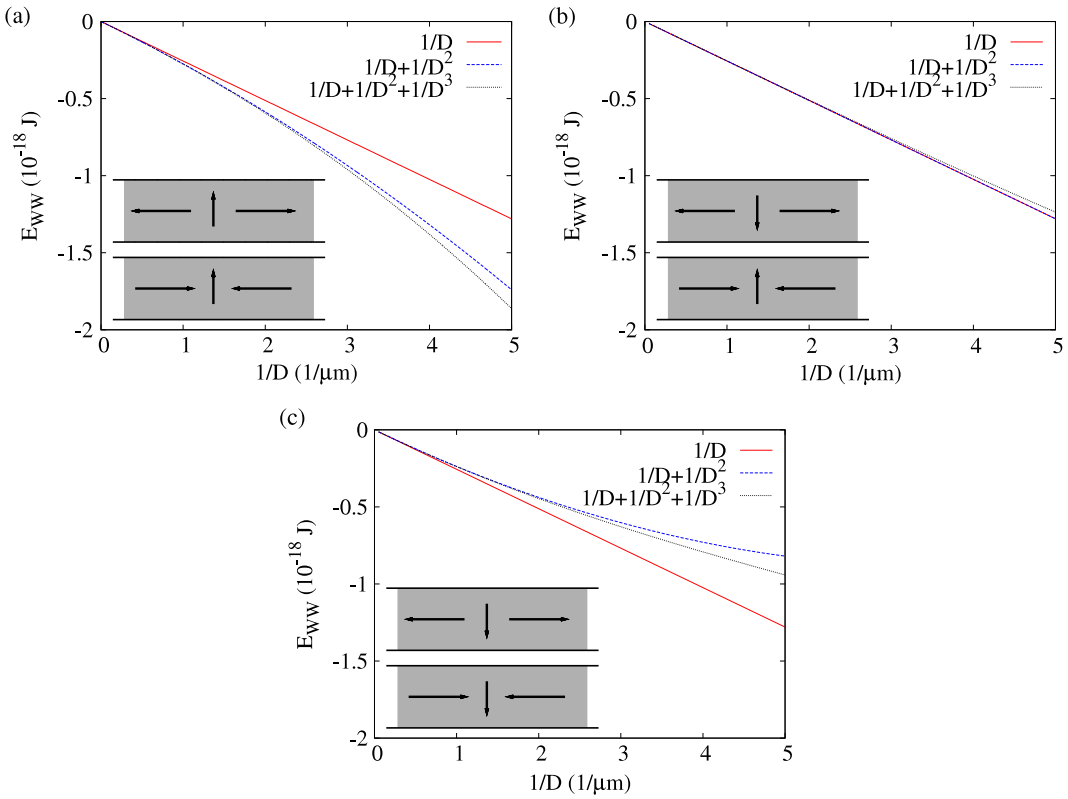

Figure 4. Interaction energy of two domain walls with $a_1a_2 = -1$ in two parallel wires with $w = 100$ nm and $d = 10$ nm calculated from equation (34) including different orders in $1/D$. The width of the domain walls is chosen as $\lambda = 22.9$ nm which is the same as for the numerical results in figure 6. The values for $a_1c_1 - a_2c_2$ are (a) $+2$, (b) 0, and (c) -2. One magnetic configuration yielding the respective values of a_1a_2 and $a_1c_1 - a_2c_2$ is shown in the inset of each subfigure.

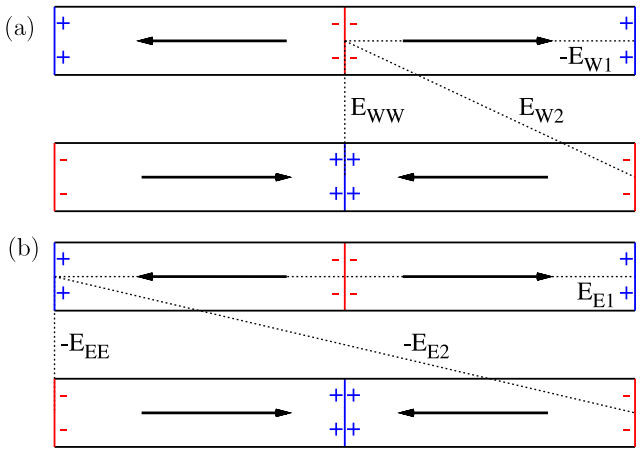

Figure 5. Scheme of the different interactions in the two wires. The positive and negative magnetic charges are denoted by blue plus signs and red minus signs, respectively. The arrows denote the magnetization in the domains. (a) Interactions between the two domain walls and between the domain walls and the ends of the wire. (b) Interactions between the ends of the wires.

bearing in mind that the magnetization at the ends of the wires is kept constant as mentioned above.

Besides the sought interaction energy of the two domain walls, the simulations also yield some additional energies that are due to the finite distance between the walls and the ends of the wires, the finite distance between two different ends, and the self-energy of the ends. The self-energies of the four wire ends and the interaction energies of adjacent ends of different wires can be calculated analytically since the magnetization at the ends of the wires is fixed. The remaining energies due to interactions with the ends of the wires decrease for longer wires. For an infinite length these interactions would vanish.

It is not possible to simulate wires of infinite length. However, it is possible to vary the length l while the distance D is kept constant. The resulting energies can now be fitted by an analytical expression that reveals the energy for very long wires. In the limit of long wires the l dependent energies can be expressed as a monopole–monopole interaction. For $a_1 = +1$, $a_2 = -1$, equation (36) becomes

$$E(l, D) = 2E_{\mathrm{W}} + E_{\mathrm{WW}}(c_1, c_2, D) - \frac{7\mu_0 M_{\mathrm{s}}^2 S^2}{2\pi l} + \frac{4\mu_0 M_{\mathrm{s}}^2 S^2}{\pi\sqrt{l^2 + 4D^2}} + \frac{\mu_0 M_{\mathrm{s}}^2 d^3}{\pi}\left(F_{\mathrm{N}}\left(\frac{w}{d}\right) + F_{\mathrm{N}}\left(\frac{D}{d}\right)\right) - \frac{\mu_0 M_{\mathrm{s}}^2 S^2}{2\pi\sqrt{l^2 + D^2}} - \frac{\mu_0 M_{\mathrm{s}}^2 d^3}{2\pi}\left(F_{\mathrm{N}}\left(\frac{D+w}{d}\right) + F_{\mathrm{N}}\left(\frac{D-w}{d}\right)\right). \quad (40)$$

Here, it is taken into account that the monopoles of the ends of the ith wire are given by $-M_{\mathrm{s}}Sa_i$.

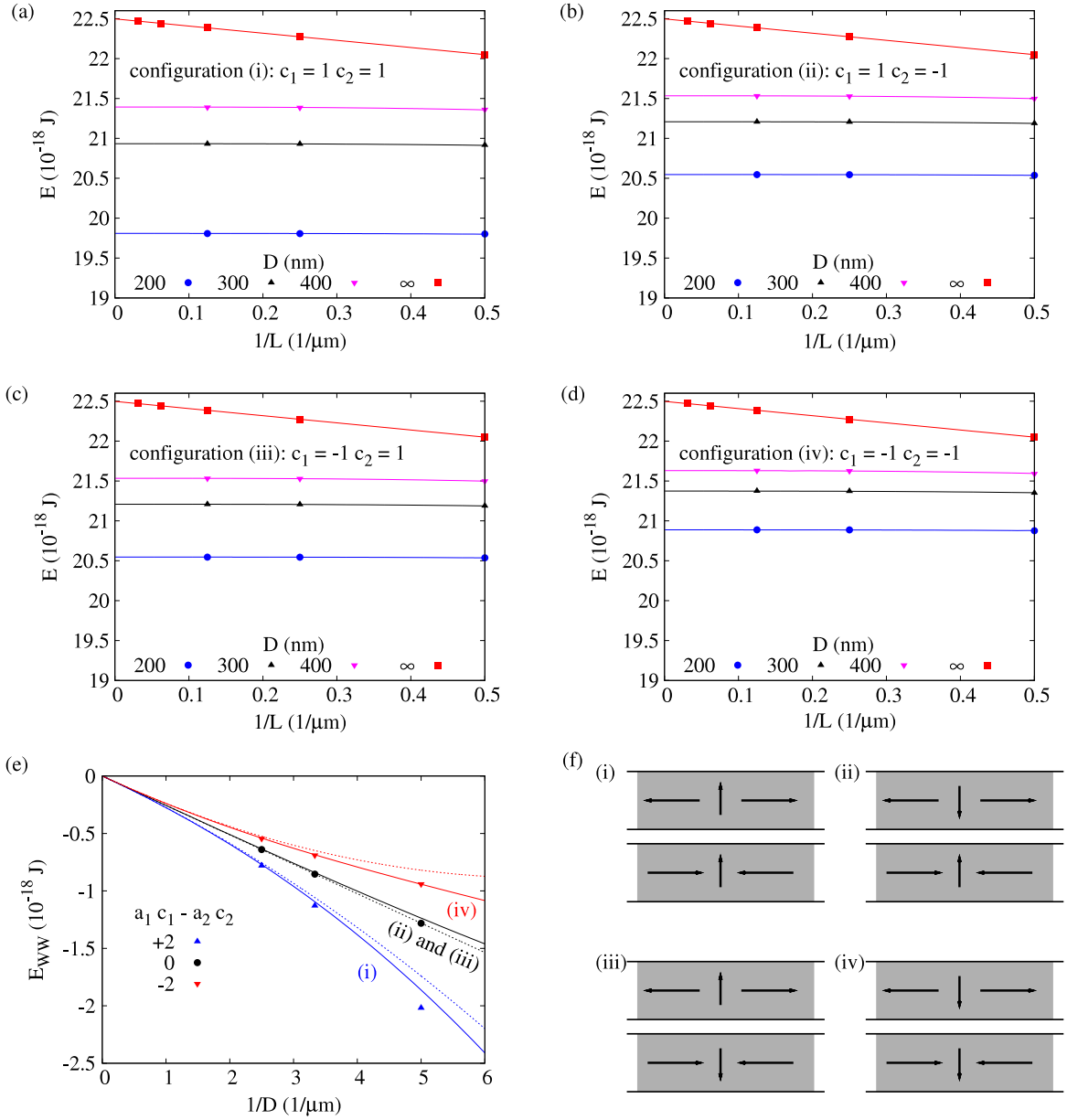

Figure 6. ((a)–(d)) Total energies of the systems shown in (f) as determined from micromagnetic simulations (dots), depending on the length L of the wires and their distance D. The lines are fits using equation (40). (e) Interaction energy of the two domain walls calculated from the fits in (a)–(d) using equation (41). The values found from (b) and (c) (both configurations have $a_1c_1 - a_2c_2 = 0$) are the same within the numerical accuracy. The solid (dashed) lines are the analytical results from equation (34) up to third (second) order in $1/D$. Here $w = 100$ nm, $d = 10$ nm, and $\lambda = 22.9$ nm have been used. The Roman numerals denote the corresponding magnetization configuration in (f). (f) Scheme of the magnetization for four different domain wall configurations with attractive interaction.

Numerically calculated energies for $a_1 = +1$ and $a_2 = -1$, and different values of c_1, c_2, D, and L are depicted in figure 6. The energies are plotted versus the inverse wire length and fitted with the asymptotic expression in equation (40) that is valid for large values of l. From this fit one fit parameter is determined. This parameter is given by the energy $E_{\mathrm{fit}}(c_1, c_2, D) = 2E_{\mathrm{W}} + E_{\mathrm{WW}}(c_1, c_2, D)$. For an infinite distance apart D of the wires the interaction energy E_{WW} certainly vanishes. This yields $E_{\mathrm{fit}}(c_1, c_2, \infty) = 2E_{\mathrm{W}}$. Thus the interaction energy of the domain walls is given by

$$E_{\mathrm{WW}}(c_1, c_2, D) = E_{\mathrm{fit}}(c_1, c_2, D) - E_{\mathrm{fit}}(c_1, c_2, \infty). \quad (41)$$

In figure 6(e) these energies are compared with the analytical result from equation (34) up to different orders in $1/D$. It can be clearly seen that the second order in $1/D$, that is the monopole–dipole interaction, is important for reproducing the behavior of the numerical data. The third order in $1/D$ is also found to be not negligible. For the configurations (ii) and (iii) the monopole–dipole interaction vanishes (see equation (34)). Thus the respective dashed line in figure 6(e) corresponds to the value of the monopole–monopole interaction only. The maximum interaction energy is found for $a_1c_1 - a_2c_2 = +2$ as predicted in equation (34). The contributions of the three

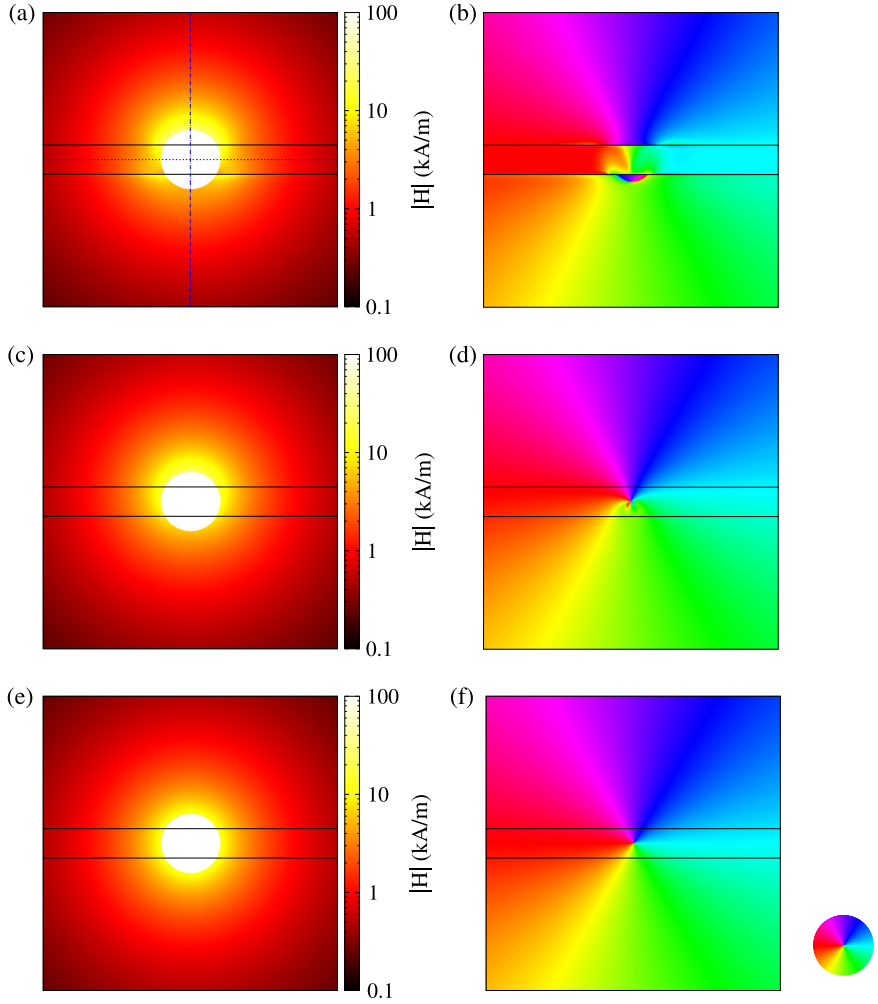

Figure 7. Top view (from the $+z$ direction) of the magnetic field that is generated by a head-to-head domain wall with $c = +1$. For the scheme of the magnetization see figure 3(a). (a) Strength of the field determined from micromagnetic simulations. (b) The angle of the field depicted in (a). ((c), (d)) Field of the same domain wall calculated from the analytically derived magnetization texture using a multipole expansion up to the third order (quadrupole). ((e), (f)) Calculated strength of the field, using the monopole only. For the sake of clarity in the illustration of the far field, which is important for the interaction with other walls, large fields in the vicinity of the wall are not shown in (a), (c), and (e). Each figure depicts an area of 1000×1000 nm^2 with the domain wall in the center. The surfaces of the wire are illustrated by solid black lines. The dashed and dashed–dotted blue lines in (a) illustrate the positions of the sections shown in figure 8.

different orders in $1/D$ to the interaction energies are plotted in figure 4.

The field that is generated by one domain wall is depicted in figures 7 and 8. It can be seen that there is a good agreement between the fields that are calculated numerically and analytically when the dipole and quadrupole moments are taken into account.

7. Conclusion

The dynamics of interacting transverse domain walls is calculated analytically making use of a multipole expansion of the interaction energy up to third order. For domain walls that are situated in different wires it is found that the main deficiency of the monopole model is the interaction of the monopole of the wall in the first wire with the dipole of the wall in the second wire and vice versa. The next order is the dipole–dipole and the quadrupole–monopole interactions. These interactions are found to be also of considerable size and non-negligible. If the two walls are in the same wire the dipole–monopole interaction vanishes and the first corrections are the dipole–dipole and the quadrupole–monopole interactions. A comparison with micromagnetic simulations shows a good agreement.

Acknowledgments

The author thanks André Drews, Stellan Bohlens, Daniela Pfannkuche, and Guido Meier for fruitful discussions and encouragement. Financial support by the Deutsche Forschungsgemeinschaft via SFB 668 ‘Magnetismus vom Einzelatom zur Nanostruktur’ and via Graduiertenkolleg 1286 ‘Functional metal–semiconductor hybrid systems’ and by the Forschungs- und Wissenschaftsstiftung Hamburg via

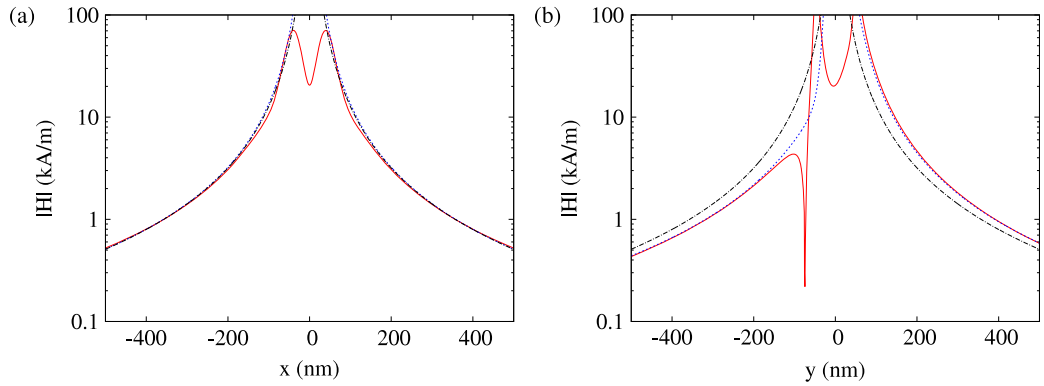

Figure 8. Sections of the magnetic field shown in figure 7. The solid red line represents the field calculated numerically. Analytical data are calculated from a multipole expansion up to the third order (dashed blue line) or using the monopole only (dashed–dotted black line). The positions of the sections in (a) and (b) are denoted in figure 7(a) by the dashed and dashed–dotted lines, respectively.

the Landesexzellenzcluster Nano-Spintronics is gratefully acknowledged.

References

[1] Berger L 1978 Low-field magnetoresistance and domain drag in ferromagnets *J. Appl. Phys.* **49** 2156
[2] Berger L 1984 Exchange interaction between ferromagnetic domain wall and electric current in very thin metallic films *J. Appl. Phys.* **55** 1954
[3] Berger L 1996 Emission of spin waves by a magnetic multilayer traversed by a current *Phys. Rev.* B **54** 9353
[4] Slonczewski J C 1996 Current-driven excitation of magnetic multilayers *J. Magn. Magn. Mater.* **159** L1
[5] Bazaliy Ya B, Jones B A and Zhang S-C 1998 Modification of the Landau–Lifshitz equation in the presence of a spin-polarized current in colossal- and giant-magnetoresistive materials *Phys. Rev.* B **57** R3213
[6] Zhang S and Li Z 2004 Roles of nonequilibrium conduction electrons on the magnetization dynamics of ferromagnets *Phys. Rev. Lett.* **93** 127204
[7] Parkin S S P, Hayashi M and Thomas L 2008 Magnetic domain-wall racetrack memory *Science* **320** 190
[8] Hayward T J, Bryan M T, Fry P W, Fundi P M, Gibbs M R J, Allwood D A, Im M-Y and Fischer P 2010 Direct imaging of domain-wall interactions in Ni80Fe20 planar nanowires *Phys. Rev.* B **81** 020410
[9] Hayward T J, Bryan M T, Fry P W, Fundi P M, Gibbs M R J, Im M -Y, Fischer P and Allwood D A 2010 Pinning induced by inter-domain wall interactions in planar magnetic nanowires *Appl. Phys. Lett.* **96** 052502
[10] Krüger B, Pfannkuche D, Bolte M, Meier G and Merkt U 2007 Current-driven domain-wall dynamics in curved ferromagnetic nanowires *Phys. Rev.* B **75** 054421
[11] Döring W 1948 Über die Trägheit der Wände zwischen Weissschen Bezirken *Z. Naturf.* **3a** 373
[12] Thomas L, Hayashi M, Jiang X, Moriya R, Rettner C and Parkin S S P 2006 Oscillatory dependence of current-driven magnetic domain wall motion on current pulse length *Nature* **443** 197
[13] Bocklage L, Krüger B, Eiselt R, Bolte M, Fischer P and Meier G 2008 Time-resolved imaging of current-induced domain-wall oscillations *Phys. Rev.* B **78** 180405
[14] Hayashi M, Thomas L, Bazaliy Ya B, Rettner C, Moriya R, Jiang X and Parkin S S P 2006 Influence of current on field-driven domain wall motion in permalloy nanowires from time resolved measurements of anisotropic magnetoresistance *Phys. Rev. Lett.* **96** 197207
[15] Mougin A, Cormier M, Adam J P, Metaxas P J and Ferr J 2007 Domain wall mobility, stability and walker breakdown in magnetic nanowires *Europhys. Lett.* **78** 57007
[16] Thomas L, Hayashi M, Jiang X, Moriya R, Rettner C and Parkin S 2007 Resonant amplification of magnetic domain-wall motion by a train of current pulses *Science* **315** 1553
[17] Bocklage L, Krüger B, Fischer P and Meier G 2010 Analytical modeling and x-ray imaging of oscillations of a single magnetic domain wall *Phys. Rev.* B **81** 054404
[18] Bocklage L, Krüger B, Matsuyama T, Bolte M, Merkt U, Pfannkuche D and Meier G 2009 Dependence of magnetic domain-wall motion on a fast changing current *Phys. Rev. Lett.* **103** 197204
[19] Donahue M J and Porter D G 1999 *OOMMF User's Guide, Version 1.0, Interagency Report NISTIR6376* (Gaithersburg, MD: National Institute of Standards and Technology) Sept. 1999 http://math.nist.gov/oommf/
[20] Newell A J, Williams W and Dunlop D 1993 A generalization of the demagnetizing tensor for nonuniform magnetization *J. Geophys. Res.* **98** 9551